scientific reports

Check for updates

OPEN

Magnetic mixed convection within wavy trapezoidal thermal energy storage systems using nano enhanced phase change material

Aissa Abderrahmane[1], Obai Younis[2], Sameh E. Ahmed[3], Abed Mourad[1], Zehba Raizha[3] & Awadallah Ahmed[4]✉

The three-dimensional (3D) MHD mixed convection mode confined 3D wavy trapezoidal enclosure is examined. The bottom plane of the trapezoidal system is irregular, particularly a wavy plane with various undulation numbers N. The forced convection phenomenon arises due to the displacement of the top region plane, whereas the porosity-enthalpy methodology characterizes the progression of charging. The heat transfer is enhanced using the nanoencapsulation phase change material (NePCM), consisting of Polyurethane as a shell and Nonadecane as a core, with water as the primary liquid base. The (GFEM) is used to treat the governing system, and a comparison between the HT (heat transmission) irreversibility and FF (fluid friction) irreversibility is performed using the function of the Be_{Avg}. The significant findings revealed that parabolic behaviors for the melting ribbon curve are given at lower values of *Re* and higher values of *Ha*. Also, reducing the undulation number is better for obtaining a higher heat transmission rate. The average Nusselt number was lowered by 60% and 19%, respectively, at the highest Reynolds number when the Hartmann number increased from 0 to 100 and N from 2 to 8. Also, the values of Re between 1 and 100 improve the heat transfer rates up to 51%.

Keywords MHD, NePCM, 3D flow, Melting, GFEM, wavy domains, lid-driven containers, irreversibility analyses

List of symbols

C_r	The ratio of heat capacity of mixture to water
C_p	Specific heat capacity (J/kgK)
f	Fusion function
g	Gravitational acceleration (m/s^2)
Gr	Grashof number
h_{sf}	Latent heat of core (J/kg)
k	Thermal conductivity (W/mK)
L	Length of the cavity (m)
l	Weight ratio of core to shell
Nu_{Avg}	Average Nusselt number
p	Pressure (Pa)
Pr	Prandtl number
r	Radius of the cylinder
Ri	Richardson number
Re	Reynolds number
T	Temperature (K)
T_{Mr}	Melting temperature range (K)
T_f	Fusion temperature (K)
V	Velocity vector (m/s)

[1]LPQ3M, University of Mascara, Mascara, Algeria. [2]Department of Mechanical Engineering, College of Engineering in Wadi Alddawasir, Prince Sattam Bin Abdulaziz University, Al kharj, Saudi Arabia. [3]Department of Mathematics, Faculty of Science, King Khalid University, Abha 62529, Saudi Arabia. [4]Department of Mechanical Engineering, Faculty of Engineering and Technology, Nile Valley University, Atbara 46611, Sudan. ✉email: awadallahahmed985@gmail.com

q_w Heat flux (W/m^2)

Greek symbols

α Thermal diffusivity (m^2/s)
β Thermal expansion coefficient (1/K)
δ Thickness of melting zone
θ Non-dimensional temperature
λ The ratio of heat capacity of NEPCM to water
μ Dynamic viscosity (kg/ms)
v kinematic viscosity (m^2/s)
v_s Volume ratio of core to shell
ρ Density (kg/m^3)
ω Angular velocity of inner cylinder (rad/s)
χ The intensity of stored energy in the core
ε Porosity

Subscript

bf Base fluid
c Core of the NEPCM
f Fusion
n Nanoparticle
m Mixture of water – NEPCM
l Liquid phase
s Shell of the NEPCM

While the need for green energy solutions grows, the need for instruments to store energy (batteries), mainly thermal energy, has grown. During the last several decades, academics in various fields have recognized the use of PCM in energy storage. Subsequently, multiple researchers have provided techniques for boosting heat transmission characteristics of PCMs-incorporated energy storage systems. They highlighted that heat transfer augmentation may be obtained by utilizing metal fins and metal foams with excellent thermal conductivity, modifying PCM's thermophysical characteristics by incorporating nanoparticles of nanoscale size[1–3] or using wavy containers due to their ability to enhance convective heat transfer and improve fluid flow characteristics. Wavy geometries are known to increase the surface area and induce secondary flow patterns, which significantly improve thermal performance in various applications[4–6].

Phase Change Materials (PCMs) uniquely absorb and release thermal energy during melting and solidification (phase change processes). These materials are pivotal in thermal energy storage, finding applications in diverse fields like electronics, building construction, and renewable energy systems[1]. The prime advantage of PCMs is their aptitude to charge and discharge large quantities of thermal energy at relatively constant temperatures, improving energy efficiency in applications like building cooling and heating[2]. However, traditional PCMs face volume expansion, corrosion, and supercooling challenges. Researchers have explored innovative techniques such as microencapsulation and nanoencapsulation to address these challenges. Microencapsulation involves enclosing PCMs within micro-sized capsules to enhance stability[3]. Nanoencapsulation takes this further, encapsulating PCMs at the nanoscale to improve surface area and stability[4].

PCMs suffer from the major drawbacks of volume growth, corrosion, and supercooling problems, and the microencapsulation of Phase Change Material was demonstrated to be a stable method to tackle these difficulties. Furthermore, it was postulated that the elevated ratio of area to volume exhibited by the micro ePCM particles could potentially raise the surface area available for heat transmission[7–9]. Li et al.[10] developed an upgraded thermal control technique using MEPCM soaked in an elevated-permeability metal foam. It was revealed that the metal assembly considerably boosted the heat transmission and decreased the time consumption to initiate phase shift. Li et al.[11] synthesized high efficiency phase change microcapsules of encapsulation. According to the TGA results, the Phase Change Material is stable up to 150 degrees Celsius. After 7560 cycles of phase changes, the enthalpy of PCM remains almost unaltered, demonstrating the MEPCM's high thermal stability and longevity. Gado[12] focused on the thermal management of electronic components using phase change materials (PCM) with triply periodic minimal surface (TPMS) structures. The major results revealed that the electronics base and cycling temperature are reduced by the presence of PCM-TPMS heat sinks substantially. Baruah et al.[13] introduced a unique macro-encapsulated PCM-metal foam hybrid system. The parametric tests indicated that the design of the metal foam is essential in defining the charging structure and the energy supply properties due to its vast net-like internal surface area. It is observed that the charging time is lowered for smaller capsule sizes, inferior permeability, and greater shell thickness. Cheng et al.[14] synthesized paraffin phase change microcapsules with a latent heat of 112.25 J/g. They evaluated the effectiveness of the thermal energy storage (TES) and the temperature regulation capabilities of the microcapsules through simulation tests. The results showed that the phase change material (PCM) effectively absorbs heat and reduces fluctuations in interior temperatures. Ho et al.[15] investigated the movement of liquid-based MEPCM through a mini channel. They discovered that the presence of the PCM capsules and other variables, such as the heat exchange fraction and liquid movement rate, affected the thermal characteristics. Eisapour et al.[16] cooled photovoltaic cells using a slurry of micro-encapsulated PCMs. The findings indicate that solar panels' operating temperatures may be effectively reduced by utilizing the slurry. Xu et al.[17] investigated a new PCM encapsulated in an ellipsoidal macrostructure. They discovered that when compared to a traditional cylindrical capsule that has a 69 mm diameter and a 750 mm length, the ellipsoidal capsule had a 60% faster discharge time but a 23% reduced storage capacity. Maier et al.[18] performed an experimental investigation on an innovative 3D-printed hollow lattice that was used to microencapsulate phase change materials and was included in mortar and lightweight mortar mixes. The findings indicated that

lattice samples achieved the minimum panel temperature during heating and significantly reduced the interior temperature. The thermal performance of cylindrically encapsulated PCM has been experimentally examined in[19]; they discovered that by increasing the HTF temperature differential and flow rate, the melting/solidification time may be decreased. Yan et al.[20] examined transient thermal energy storage capabilities of a segmented cavity loaded with MEPCM. Their findings demonstrated increased net energy storage in a cavity with a lower aspect ratio. Regrettably, several researchers found that the MEPCM particles' residual poor thermal conductivity and contact thermal resistance subsequently culminated in low heat dissipation rates[21].

Recently, a novel form of PCM encapsulation using nanoparticles has garnered substantial interest due to the advantages of a larger surface area fraction, a steadier solution, and a reduced break probability when compared to microparticle-sized PCM capsules. Current research has concentrated on the production technologies and thermal features of various nano-NePCMs for thermal energy storage Utilization[22–24]. Li et al.[25] established a novel, stable, and efficient design for free thermal systems by integrating the nano-capsulated PCM slurry soaked in metal foams. The authors discovered that this recently developed nano/foam-phase change material combination improves heat transfer efficiency while reducing convection coefficient dependency. In[26], authors explored the influence of wing inclination on the free convective flow of aqueous-based NePCMs inside a heat exchanger fitted with wing-shaped fins. The results indicate that the direction of the fins improves thermal behavior in comparison to horizontal fins. Zadeh et al.[27] examined the conjugate free convective flow and entropy production inside a square enclosure. The authors found that incorporating NePCMs into the base liquid boosted the heat transmission rate by about 45%, albeit it raised the Bejan number. Ghalambazet al.[28] examined the heat transmission of NePCM over a vertical surface. The findings demonstrated that heat transport is enhanced by decreasing the melting temperature of NePCMs. Ahmed et al.[29] numerically examined radiative and convective heat transfer fluid flow passing through a prismatic cage. The authors considered Nonadecane to be NePCM core and shell material, respectively. The findings reveal that the application of NePCM greatly improves heat transmission. Sadr et al.[30] explored the mixed convective motion of water and NePCM within a square chamber with a spinning heated cylinder. They observed that Increasing the strength of stored energy (χ) in the core has a detrimental impact on Nu (the Nusselt number). Agrestiet al.[31] developed a novel solvent-assisted technique to generate emulsions of NePCM paraffin in water. The data reveal that the thermal capacity of water rose by up to 40%, and the undercooling was lowered to 2 °C. Heydarianet al.[32] explored the thermal effectiveness of a heat pipe filled with a suspension of NePCM water. The NePCM suspension was shown to improve heat transmission and decrease the thermal resistance of a pulsing heat tube. Ghalambazet al.[33] created a model of NePCMs suspended in a cylindrical container. They discovered that NePCM particles' latent heat has a significant contribution to energy storage as general and heat transport and so their fusion temperature may be used to adjust the thermal behavior. An eccentric annulus cavity loaded with a suspension of NePCMs was examined in[34,35]. The findings illustrate the outcome of the phase change core of particles on heat transmission rate enhancement, as well as the relationship between these effects and the melting temperature, the volumetric percentage of NePCM particles, and the Stefan number.

Several researchers have addressed the magnetic field impact on the charging and discharging of NePCMs. Zhuang et al.[36] experimentally visualized the charging process of NePCM inside a porous cavity subjected to a non-uniform magnetic field. The impacts of NePCM nanoparticle concentration, filling arrangement of metal foam, and magnetic field direction were addressed. The findings indicated that using nanoparticles reduced charging time by 29.32% and increased energy storage by 0.26%. Positioning the irregular magnetic field on the right side resulted in increasing melting time by 19.59% and energy storage by 2.45%. Sheikhoeslami[37] numerically investigated the discharging of NePCM within a permeable energy storage enclosure subjected to a magnetic field. The Hartmann number and nanoparticle volumetric fraction impact on the solidification time and stored energy are presented and discussed. The study concluded that augmentation of the Hartmann number reduced the solidification time and increased the energy stored. Xu et al.[38] numerically explored the effect of a magnetic field on NePCM charging inside a porous cubical chamber. The authors also studied the implications of nanoparticle volumetric fraction, Rayleigh number, and the magnetic number of the melting process. The results revealed that increasing nanoparticle volumetric fraction and Rayleigh number enhanced the stored energy. Moreover, at relatively low Rayleigh, the magnetic field-driven convection has a positive effect on the charging process. Shi et al.[39] performed a computational analysis examining the fusion and solidification progressions of nano-encapsulated PCM within a shell and a multi-pipe thermal energy storage system subjected to a magnetic field. Their results revealed that increasing the magnetic field intensity reduced the fusion and solidification time by 80.02% and 53.19%, respectively.

In the context of existing literature, our research introduces a system modeling focusing on three-dimensional (3D) mixed magnetohydrodynamic (MHD) convection inside a corrugated (3D) trapezoidal enclosure. The novelty of this study appears in combining the three-dimensional domain having an irregular corrugated bottom plane with variable corrugation numbers (N) and forced convection via displacement of the upper side in the presence of a Lorentz force. To the best of the author's knowledge, this distinct configuration has not been studied in previous literature. While previous research has primarily concentrated on enhancing heat transmission characteristics through methods like metal fins, metal foams, and modified thermophysical properties of PCMs adopting nanoparticle utilization, the current study introduces a novel approach by employing nanoencapsulation. The integration of Polyurethane and Nonadecane as shell and core respectively, with a primary liquid base of water, stands as a novel contribution, particularly when contrasted with conventional methods. Overall, this research is marked by the introduction of a unique 3D corrugated trapezoidal enclosure and the use of nanoencapsulation to enhance heat transfer. The novelty of this study, in comparison with the existing literature, highlights its contribution to the understanding and application of fluid dynamics and thermal energy storage systems.

Description of the physical model

The forced convective flow of a nanoliquid and particles of a nanoencapsulation PCM (NePCM) is studied in trapezoidal-shaped cavities with a wavy bottom wall. Figure 1 depicts the structural configuration of the enclosure under investigation, featuring a top wall that is driven by a lid.

The titled side edges are isothermal and have cold temperatures of Tc, while T_h is the temperature of the wavy bottom hot wall. The upper wall is moving in the positive x-direction at a steady velocity of U_0. Imposed a homogenous magnetic field. It is widely postulated that the impact of movement currents, viscous dissipation, and radiation are negligible[41,43]. The Boussinesq approximation is commonly applied to model-free convection. The density of nanoliquids remains unaffected by alterations in pressure. Temperature differentials, conversely, modify the density. The nano-additives are homogeneously dispersed within the host fluid, resulting in the establishment of dynamic and thermal equilibrium between the two components. The shape (Trapezoidal containers with wavy bottom boundary) was chosen for two reasons: the first because of the lack of research on it, and second, its side walls are inclined, and this facilitates the movement of the flow near them.

Governing formulations

Besides the assumptions mentioned earlier, the three-dimensional flow is steady and laminar, and the suspension is incompressible. The gravity effect is in the normal direction, and both the forced and free convection modes are assumed. The suspension has the components water and NePCM. Also, the well-known Boussinesq relation is applied for the mixture density. The following equations describe continuity, momentum, and energy[40,41]:

$$\partial_x u + \partial_y v + \partial_z w = 0 \tag{1}$$

$$\mu_m \left(\frac{\partial^2 u}{\partial x^2} + \frac{\partial^2 u}{\partial y^2} + \frac{\partial^2 u}{\partial z^2}\right) - \rho_m \left(u\frac{\partial u}{\partial x} + v\frac{\partial u}{\partial y} + w\frac{\partial u}{\partial z}\right) - \frac{\partial p}{\partial x} - \sigma_m B_0^2 u = 0 \tag{2}$$

$$\mu_m \left(\frac{\partial^2 v}{\partial x^2} + \frac{\partial^2 v}{\partial y^2} + \frac{\partial^2 v}{\partial z^2}\right) - \rho_m \left(u\frac{\partial v}{\partial x} + v\frac{\partial v}{\partial y} + w\frac{\partial v}{\partial z}\right) - \frac{\partial p}{\partial y} - \sigma_m B_0^2 v = 0 \tag{3}$$

$$\mu_m \left(\frac{\partial^2 w}{\partial y^2} + \frac{\partial^2 w}{\partial y^2} + \frac{\partial^2 w}{\partial z^2}\right) - \rho_m \left(U\frac{\partial w}{\partial x} + v\frac{\partial w}{\partial y} + w\frac{\partial w}{\partial z}\right) - \frac{\partial p}{\partial y} + g\rho_{bf}\beta_{bf}(T - T_\infty) = 0 \tag{4}$$

$$\left(u\frac{\partial}{\partial x}(\rho_m CpT) + v\frac{\partial}{\partial y}(\rho_m CpT) + w\frac{\partial}{\partial z}(\rho_m CpT)\right) = k_{bf}\left(\frac{\partial^2 T}{\partial x^2} + \frac{\partial^2 T}{\partial y^2} + \frac{\partial^2 T}{\partial z^2}\right) \tag{5}$$

Where x, y, z are Cartesian coordinates, and the dimensional quantities are velocities u, v, w, temperature T, pressure p, thermal expansion β, density, gravity g, and the dynamic viscosity μ. The subscript b states the suspension bulk characteristics.

By specifying the non -dimensional parameters below:

$$X = \frac{x}{L},\ Y = \frac{y}{L},\ W = \frac{w}{L},\ U = \frac{u}{U_0},\ V = \frac{v}{U_0},\ W = \frac{w}{U_0},\ \theta = \frac{T - T_c}{T_h - T_c},,\ P = \frac{p}{\rho_f (U_0)^2}, \tag{6}$$

We may render the governing equations dimensionless[40,41]:

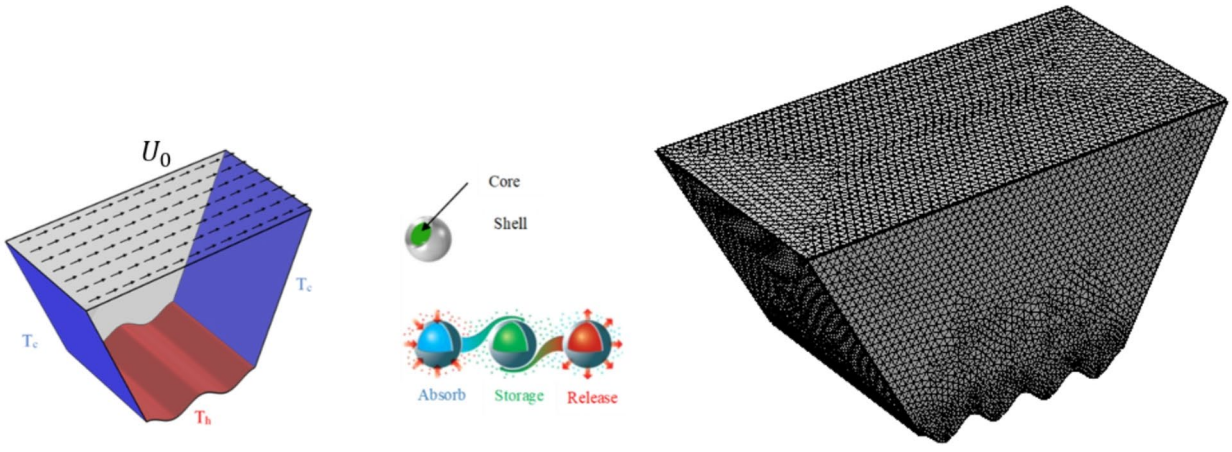


Fig. 1. Physical problems and mesh [MATLAB software, R2024b, Number of Licenses, 12562671, https://www.mathworks.com/licensecenter/trials/12562671/products].

$$\frac{\partial U}{\partial X}+\frac{\partial V}{\partial Y}+\frac{\partial W}{\partial Z}=0 \tag{7}$$

$$\frac{1}{Re_{bf}}\left(\frac{\mu_m}{\mu_{bf}}\right)\left(\frac{\partial^2 U}{\partial X^2}+\frac{\partial^2 U}{\partial Y^2}+\frac{\partial^2 U}{\partial Z^2}\right)-\left(\frac{\rho_m}{\rho_{bf}}\right)\left(U\frac{\partial U}{\partial X}+V\frac{\partial U}{\partial Y}+W\frac{\partial U}{\partial Z}\right)-\frac{\partial p}{\partial X}-\frac{\sigma_m}{\sigma_{bf}}\frac{Ha^2}{Re_{bf}}U=0 \tag{8}$$

$$\frac{1}{Re_{bf}}\left(\frac{\mu_m}{\mu_{bf}}\right)\left(\frac{\partial^2 V}{\partial X^2}+\frac{\partial^2 V}{\partial Y^2}+\frac{\partial^2 V}{\partial Z^2}\right)-\left(\frac{\rho_m}{\rho_{bf}}\right)\left(U\frac{\partial V}{\partial X}+V\frac{\partial V}{\partial Y}+W\frac{\partial V}{\partial Z}\right)-\frac{\partial p}{\partial Y}-\frac{\sigma_m}{\sigma_{bf}}\frac{Ha^2}{Re_{bf}}V=0 \tag{9}$$

$$\frac{1}{Re_{bf}}\left(\frac{\mu_m}{\mu_{bf}}\right)\left(\frac{\partial^2 W}{\partial X^2}+\frac{\partial^2 W}{\partial Y^2}+\frac{\partial^2 W}{\partial Z^2}\right)-\left(\frac{\rho_m}{\rho_{bf}}\right)\left(U\frac{\partial W}{\partial X}+V\frac{\partial W}{\partial Y}+W\frac{\partial W}{\partial Z}\right)-\frac{\partial p}{\partial Y}+\frac{Gr_{bf}}{\rho_{bf}Re_{bf}^2}\left(\frac{(\rho\beta)_m}{(\rho\beta)_{bf}}\right)\theta=0 \tag{10}$$

$$\left(U\frac{\partial}{\partial X}(Cr\theta)+V\frac{\partial}{\partial Y}(Cr\theta)+W\frac{\partial}{\partial Z}(Cr\theta)\right)=\frac{1}{Re_{bf}Pr_{bf}}\left(\frac{k_m}{k_{bf}}\right)\left(\frac{\partial^2\theta}{\partial X^2}+\frac{\partial^2\theta}{\partial Y^2}+\frac{\partial^2\theta}{\partial Z^2}\right) \tag{11}$$

Where X, Y, Z are the dimensionless coordinates, U, V, W are the dimensionless velocity, and θ is the dimensionless temperature. The non-dimensional numbers associated with the problem read[40]:

$$v_{bf}=\frac{\mu_{bf}}{\rho_{bf}}, \alpha_{bf}=\frac{k_{bf}}{(\rho c_p)_{bf}}, Pr=\frac{v_{bf}}{\alpha_{bf}}, Re_{bf}=\frac{U_0 L}{v_{bf}}, and\ Gr_{bf}=\frac{g\beta_{bf}\Delta T L^3}{v_{bf}^2}. \tag{12}$$

Additionally, the non-dimensional number (Cr) in the energy equation represents the heat capacity ratio of the mixture to the base fluid.

$$Cr=\frac{(\rho C_P)_m}{(\rho C_P)_{bf}}=1-\phi+\lambda\phi+\frac{\phi}{\chi}f \tag{13}$$

Where λ is the latent heat of the NePCM core and could be determined by applying Eq. (14).

$$\lambda=\frac{\left(C_{p_{c,1}}+lC_{p_s}\right)\rho_c\rho_s}{(\rho_s+l\rho_c)(\rho C_P)_{bf}} \tag{14}$$

Furthermore, Eq. (7) defines χ as the quotient of the increase in base liquid temperature and the energy retained as core latent heat.

$$\chi=\frac{C_{P,bf}}{h_{sf}/T_{Mr}}\frac{\rho_{bf}(\rho_s+l\rho_c)}{(\rho_s\rho_c)} \tag{15}$$

Moreover, in Eq. (7) f represents the fusion function and could be obtained as in Eq. (16).

$$f=\frac{\pi}{2}sin\left(\frac{\pi}{\delta}\left(\theta-\theta_f+\frac{\delta}{2}\right)\right)\times\begin{cases}0 & \theta<\theta_f-\frac{\delta}{2}\\ 1 & \theta_f-\frac{\delta}{2}<T<\theta_f+\frac{\delta}{2}\\ 0 & \theta>\theta_f+\frac{\delta}{2}\end{cases} \tag{16}$$

Where:

$$\delta=\frac{T_{Mr}}{\Delta T},\ and\ \theta_f=\frac{T_f-T_C}{\Delta T}$$

Here, T_f is the fusion temperature where the temperature nanoliquid is higher than the charging point of the NePCM core $\left(T>T_f+\frac{T_{Mt}}{2}\right)$ or less than the core solidification temperature $\left(T<T_f-\frac{T_{\Delta u}}{2}\right)$, the final term of Eq. (9) equals 0, and the Cr values reduce.

Local (Nu_{loc}) and Average (Nu_{Avc}) Nusselt numbers read:

$$Nu_{loc}=\frac{k_m}{k_{bf}}\frac{\partial\theta}{\partial n},\ Nu_{Ave}=\frac{1}{S}\int_0^L\int_0^L Nu_{loc}(s)\,ds \tag{17}$$

The local entropy generation pace consists of the thermal and frictional entropy generation rates, which are represented by Eqs. (8) and (9), correspondingly[45,46]:

$$S_f'''=\frac{\mu}{T}\left\{2\left[\left(\frac{\partial v_x}{\partial x}\right)^2+\left(\frac{\partial v_y}{\partial y}\right)^2+\left(\frac{\partial v_z}{\partial z}\right)^2\right]+\left(\frac{\partial v_x}{\partial y}+\frac{\partial v_y}{\partial x}\right)^2+\left(\frac{\partial v_z}{\partial x}+\frac{\partial v_x}{\partial z}\right)^2+\left(\frac{\partial v_y}{\partial z}+\frac{\partial v_z}{\partial y}\right)^2\right\}+\frac{\sigma_m\beta_0^2}{T_0}[\boldsymbol{J}\times\boldsymbol{B}]^2 \tag{18}$$

$$S_T'''=\frac{k}{T^2}\left[\left(\frac{\partial T}{\partial x}\right)^2+\left(\frac{\partial T}{\partial y}\right)^2+\left(\frac{\partial T}{\partial z}\right)^2\right] \tag{19}$$

The global entropy generation pace of the full area is determined as the integral of the local rates across the whole domain (Eqs. (20) and (21)):

$$\dot{S}_f = \int_V S_f''' \, dV \tag{20}$$

$$\dot{S}_T = \int_V S_T''' \, dV \tag{21}$$

Characteristics of NePCM-water suspension:

The nano-encapsulated PCM comprises a nonadecane core that is enveloped by a polyurethane shell. Table 1 shows the thermophysical factors of the constituents utilized in the production of the nano-additives and the basic liquid.

The thermodynamic characteristics of NePCM can be analyzed by taking into account the features of both the core and the thermophysical shell, as outlined below:

$$\rho_n = \frac{(1+l)\rho_c \rho_s}{\rho_s + l\rho_c} \tag{22}$$

Moreover, it should be noted that the specific heat capacity of the NePCM core, denoted as $C_{p,c}$, exhibits certain characteristics within the temperature interval between the phase change:

$$C_{p,c} = C_p c, t + \left\{ \frac{\pi}{2} \left(\frac{h_{sf}}{T_{Mr}} - C_{pc,l} \right) \left(sin\pi \, \frac{T - (T_f - T_{Mr}2)}{T_{Mr}} \right) \right\} = \begin{cases} 0 & if\, T < T_f - \frac{T_{Mr}}{2}, \\ 1 & if\, T_f - \frac{T_{Mr}}{2} < T < T_f + \frac{T_{Mr}}{2}, \\ 0 & if\, T < T_f + \frac{T_{Mr}}{2} \end{cases} \tag{23}$$

Details about specific heat capacity in addition to the thermal expansion factor of the NePCM read[40]:

$$C_{p,n} = \frac{(C_{p,c} + lC_s)\,\rho_c \rho_s}{(\rho_s + l\rho_c)\,\rho_n}, \quad \beta_n = \beta_c + \left(\frac{\beta_s - \beta_c}{2} \right) \left(1 - \frac{l\rho_s}{\rho_c} \right) \tag{24}$$

The mixture's thermophysical equations read[40].

$$\rho_m = (1-\phi)\,\rho_{bf} + \phi\,\rho_n, \quad C_{P_m m} = \frac{(1-\phi)\rho_f C_{Pbf} + \phi\,\rho_n C_{P,n}}{\rho_m} \tag{25}$$

$$\beta_m = \frac{(1-\phi)\rho_{bf}\beta_{bf} + \psi\,\rho_n \beta_n}{\rho_m} \tag{26}$$

Where the subscript m denotes the mixture, n denotes NePCM, denotes the core, and the shell is denoted by the subscript s. The current work considers the volumetric fraction constant at 0.035. Hence, the dynamic viscosity of the mixture equals $122 \times 10^{-5} kg/m.s$ and thermal conductivity equals $0.7\, W/m.K$ at $303\, K$[32].

Grid sensitivity test and verification

The present investigation was performed by using the finite element method (FEM) to solve the partial differential equation (PDE). The algorithm used for that is called the Galerkin-finite element approach. The working principle of this numerical simulator is to convert that set of PDE into a matrix system. Then, using the initial boundary conditions, the Galerkin-finite algorithm solves the matrix system to determine a solution. The size of the matrix is related to the density of the elements forming the grid mesh.

Table 2 illustrates the mesh sensitivity test findings. For the mesh sensitivity examination, the Nusselt number on the hot surface at (Re of 100, Ha of 0, Ø of 4%, and $N=4$) were used. The results show that the grid size is **23,362**. To verify the current findings, the outcomes generated by the utilized model in the present work are compared with those documented in Rashed et al.'s previous research[42]., as shown in Fig. 2. It is noted through the comparison results illustrated in Fig. 2 that there is a clear similarity in the results. This note indicates the accuracy of the method used in the present investigation. Also, a comparison between the average Nusselt number value of the utilized model and that of Ghalambaz et al.'s work[41] is presented in Table 3.

	Material	$\beta\ (K^{-1})$	$C(kJ/kgK)$	$k(W/mK)$	$\rho\ (kg/m^3)$
Core	Nonadecane	17.28×10^{-5}	1.3177		786
Shell	Polyurethane		2.037		721
Base fluid	Water	21×10^{-5}	4.179	0.613	997.1

Table 1. Thermophysical characteristics of NePCMs and base fluid[43].

No. of elements	1632	2302	3486	8987	23,362
Ψ_{max}	-33.782	-33.736	−33.714	-33.673	**-33.673**
Nu_a	7.8673	7.8078	7.8990	7.8817	**7.8815**

Table 2. Grid independence test at re = 100, ha = 0, Ø =4%, and $N = 4$.

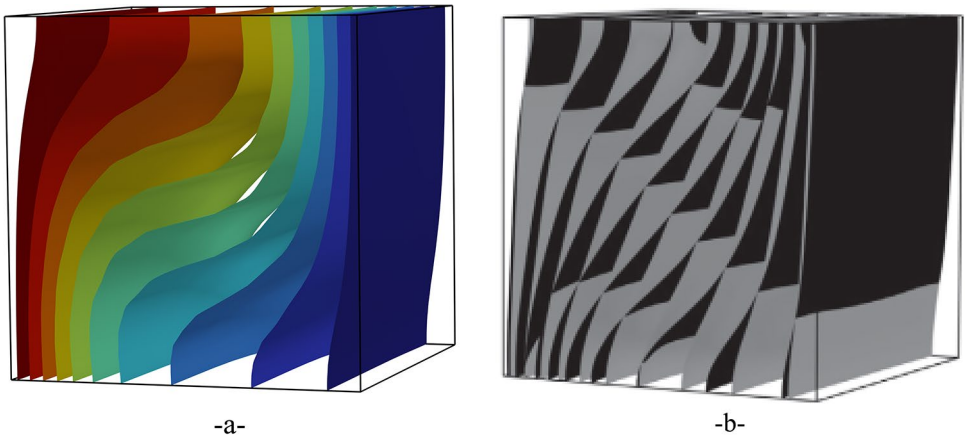


Fig. 2. Comparison of present work (**a**) with that of literature (**b**) for Ra = 10^5 and Ha = 100[42].

Ra	Ghalambaz et al.[41]]	Present model
10^5	4.7206	4.7214
10^6	9.2197	9.2220

Table 3. Comparison of Nu_{avg} at the hot wall evaluated by the present model and those reported in Ghalambaz et al.'s work[41] for Ø = 0 and pr = 6.2.

Results and discussion

A three-dimensional complex plane is considered. Here, an irregular wavy plane is assumed as a bottom boundary with the undulation number $N\ (1 \leq N \leq 4)$. Also, the mixed convection is characterized by the values of the Reynolds number Re, which has the range $(1 \leq Re \leq 500)$. Furthermore, wide ranges for the Hartmann number Ha and nanoparticles volumetric fraction φ are taken into account; those are $0 \leq Ha \leq 100$ and $0\% \leq \varphi \leq 8\%$, respectively. All these computations are carried out at $T_f = 0.35$.

Figure 3 illustrates the features of the streamlines ψ, iso-surfaces θ and melting case S for dissimilar values of the Reynolds number Re. At the low values of Re ($Re \leq 1$), the streamline features are weak, and their values are small. Also, the iso-surfaces show that the conduction mode is dominant, while a parabolic behavior for the melting case is given. Here, the stream function maximum values are about 80, 800, and 4000 at Re=10, 100, and 500, respectively, which can be approximated as $\psi_{max} = 8 * Re$. Additionally, the features of the temperature point to a higher rate of heat transfer are given as Re is increased. Moreover, the melting features show a strip curve obtained within a 3D flow area; this curve moves towards the upper plane as Re is increased. Physically, these features are due to the improvements in the forced flow resulting from the upper plane movements that is increases as Re is growing.

Figure 4 illustrates the impacts of the undulation number $N\ (1 \leq N \leq 4)$ on the behaviors of the streamlines, temperature, and melting features at $Re = 100$, for all values of N, a major forced eddy is seen within the motion area. Also, the temperature distributions are gathered near the isothermal planes (left, right, and bottom planes), and the melting behaviors follow the temperature behaviors for all values of N. The alteration of the undulation number N causes the forced and mixed convection modes to be reduced. Here, the flow recirculation and temperature gradients near the bottom boundaries diminish as N is increased. From the physical aspect, the rise in N results in more complexity in the flow domain; hence, more obstruction is given for the nanoliquid flow.

The features of the streamlines ψ, iso-surfaces θ and melting behaviors S for various values of Ha are depicted in Fig. 5. Here, the increase in Ha causes a reduction in the flow features, temperature distributions, and melting process. The physical interpretation of this behavior is due to the well-known Lorentz force, which obstructs the mixed convection mode. Unlike the Ha impacts on flow features, heat transfer, and melting situation, the increment in φ (the nanoparticles volume fraction) results in a clearer enhancement in the values of the streamlines. At the same time, the temperature distributions are less affected. Through Figs. 3 and 4, and

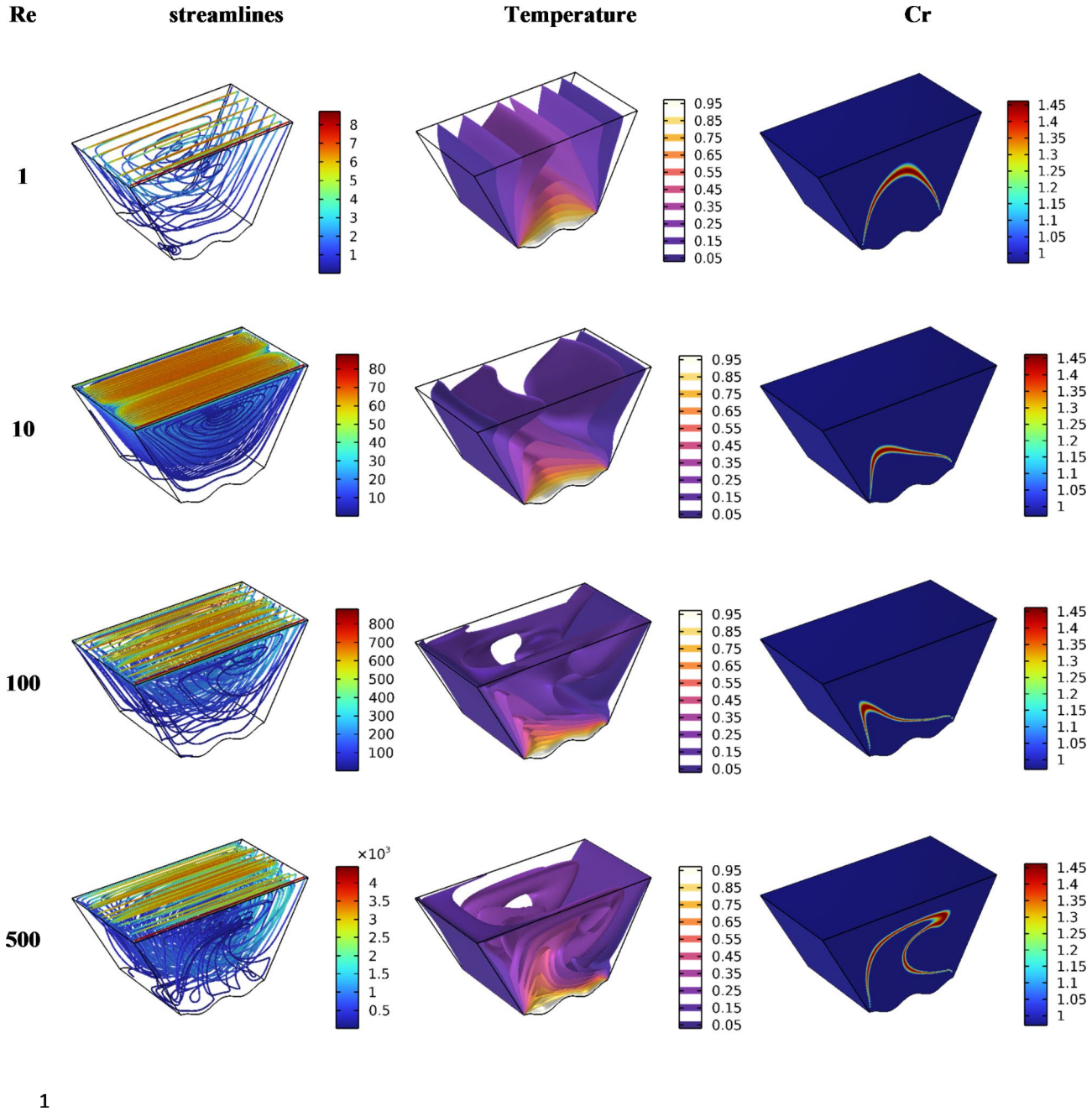


Fig. 3. Impacts of Re coefficient on streamlines, iso-surfaces, and heat capacity ratio for $Ha = 0$, and φ = 0.04 [MATLAB software, R2024b, Number of License, 12562671, https://www.mathworks.com/licensecenter/trials/12562671/products].

5, it is clear that the speed of the movement inside the room is mainly related to the movement speed of the upper wall; that is, the higher the latter, the greater the fluid withdrawal, which raises the speed of the flow. As for the magnetic field, it induces a reduction in the velocity of the flow due to the Lorentz force arising here. As for the corrugated bottom of the room, it is noted that the number of waves at the bottom does not affect the general behavior of the fluid and thermal diffusion. These observations do not contract what has been previously understood[44–48].

These influences are illustrated in Fig. 6, which reveals that there is no melting situation at $\varphi = 0$. However, as φ is altered, the melting process becomes significant due to the increment in the concentration of PCM within the flow domain. The transmitted heat rate is represented here with values of the average Nusselt coefficient. This tool is examined under the variations of Re, Ha, and the nanoparticles volume fraction φ and presented in Fig. 6. The figure revealed that increasing Re leads to enhancements in spite of the variations of the other considered parameters. This means that there is an important effect of φ and N on it. This behavior is due to the increase in forced convection, which leads to the transfer of a large amount of heat to the working fluid. On the

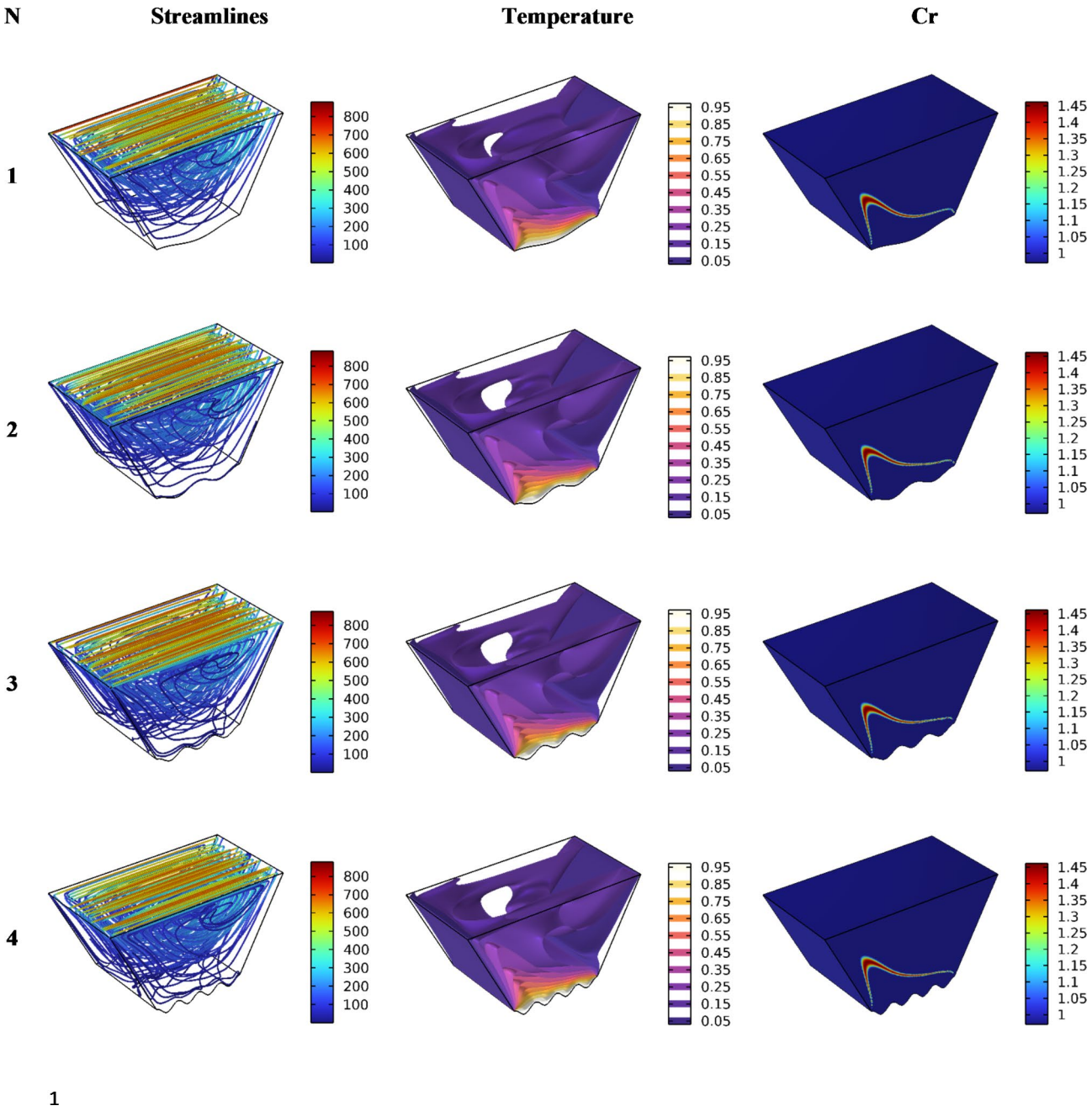


Fig. 4. N influence on streamlines, iso-surfaces, and heat capacity ratio for Re = 100, and φ= 0.04, $Ha = 0$ [MATLAB software, R2024b, Number of License, 12562671, https://www.mathworks.com/licensecenter/trials/12562671/products].

contrary, the Lorentz above force and complexity of the domain cause a reduction in the temperature gradients, and therefore, the increase in Ha and N causes a significant diminishing in Nu_{avg}.

In discussion of Fig. 7, it should be mentioned that the comparison between heat transmission irreversibility and fluid friction irreversibility can be performed using the Bejan number Be_{avg} values. In Fig. 7, the values of Be_{avg} under the variations of N, Re, φ, and Ha are presented. It is noticeable that all the values of Re greater than 50 cause a dominance in FF (Fluid Friction) entropy compared to the heat transmission entropy. As well, the values of Be_{avg} are less affected by the variations of N and φ, while the increase in Ha causes a clear reduction in Be_{avg}. From the physical view, the increase in Ha causes an improvements in the gradients of the velocity which enhances the fluid friction irreversibility compared to the heat transfer irreversibility and hence Be_{avg} is reduced. In addition to this, it is noted that the factor Be_{avg} is affected a lot in terms of Ha, and its effect is almost non-existent in terms of N and φ, because we noticed the presence of Lorentz force in terms of Ha number, which affects the movement of the fluid, which leads to a change in the flow of thermal energy, and this affects the factor Be_{avg}. Also, from this figure, and since the Be_{avg} is the ratio of the heat transfer

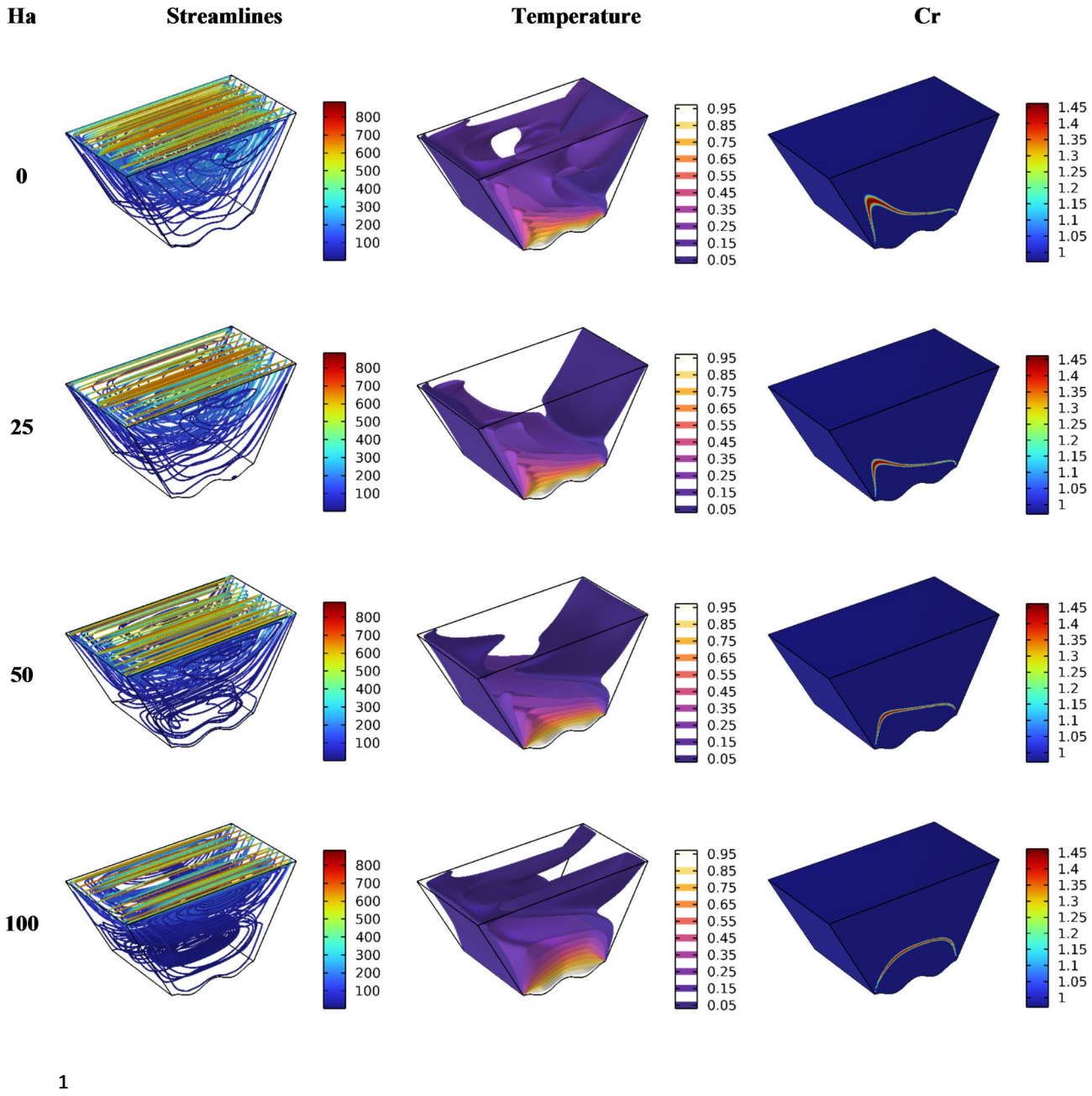


Fig. 5. Hartmann number effect on streamlines, iso-surfaces, and heat capacity ratio for Re = 100, $N = 2$, and $\varphi = 0.04$ [MATLAB software, R2024b, Number of License, 12562671, https://www.mathworks.com/licensecenter/trials/12562671/products].

entropy and total entropy generation, the impacts of the governing parameter on these tools can be deduced. It can be noted that the increase in Re values causes a decrease in the fluid friction entropy while the heat transfer entropy is enhanced. Additionally, the growth in Ha causes an increase in the total entropy generation due to the rise in the velocity gradients. Furthermore, the alteration in the φ causes an increment in the gradients of the temperature, and hence, the heat transfer entropy is improved. This behavior is similar to that elicited in the previous works[44–48].

Conclusion

The three-dimensional charging process of NePCM within a 3D wavy trapezoidal cavity has been examined. The motion and transmitted heat occur due to the movement of the upper plane together with a constant temperature condition at the lower wavy plane. The temperature differences were obtained by assuming the inclined side planes are cold. The GFEM is utilized to address the governing system., and the enthalpy-porosity approach was employed to simulate the charging situation. The present study leads to the following major outcomes:

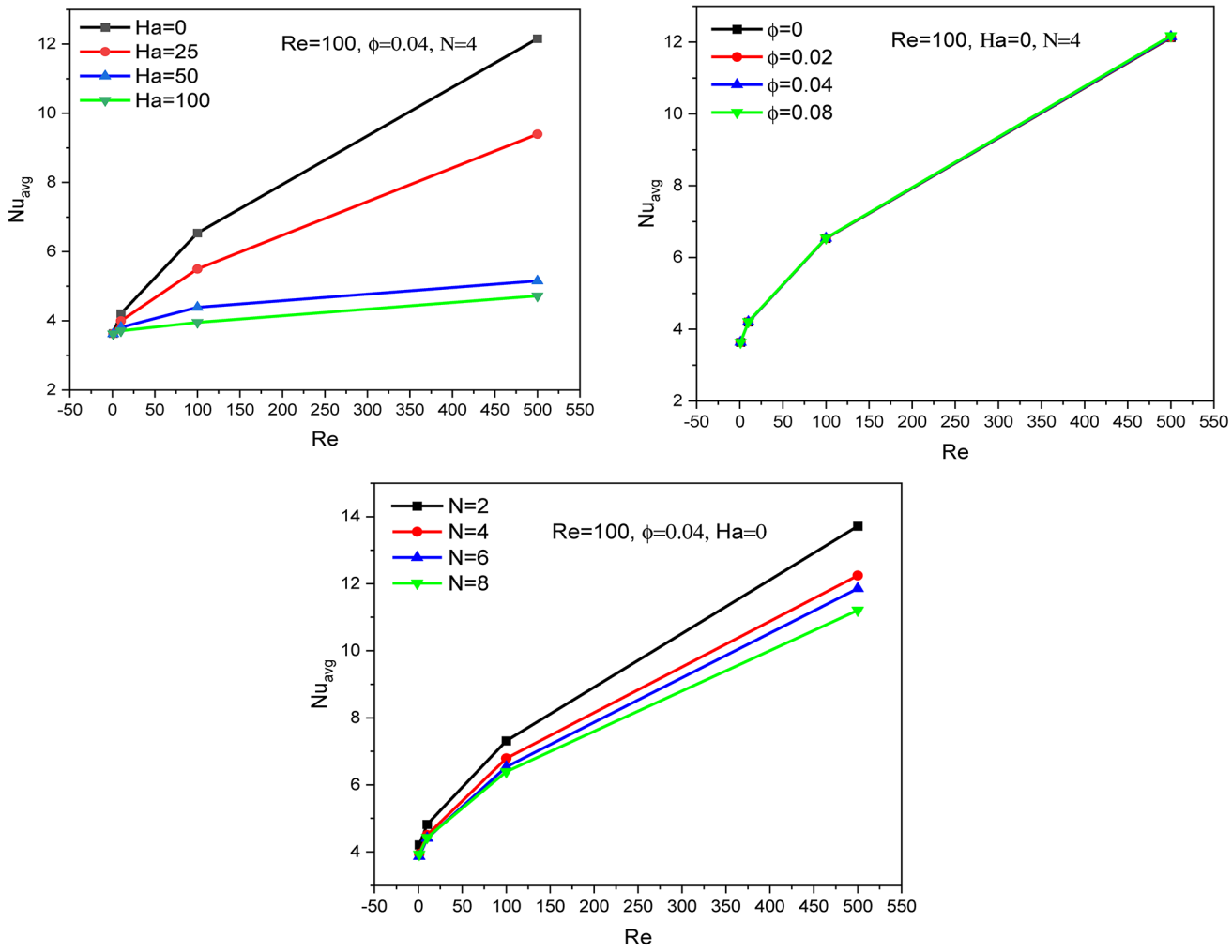


Fig. 6. Impact of the variations of Re, Ha, and φ on Nu $_{avg}$.

- Results show that the values of the streamlines are highly dependent on Re and indicate a good correlation with $\psi_{max} = 8 * Re$.
- The values of Ha between 0 and 100 gives a reduction in the heat transfer rate up to 60% while the alteration in Re gives some improvements in the Nusselt number by 51%.
- The melting behaviors follow the temperature behaviors, and their illustrative features are noted at the low values of Re and higher values of Ha.
- The value $\varphi = 0$, leads to the disappearance of the melting ribbon curve.
- The increase in Ha and N causes a reduction in the temperature gradients and hence Nu_{avg} are diminishing.
- The values $Re > 50$ cause a dominance of FF irreversibility.
- The alteration in Ha results in a decrease in the velocity gradients, and hence the Be_{avg} is diminishing.
- The presented results indicated that Ha has a significant influence on Be_{avg} while the remaining factors (φ and N) were not highly affected Be_{avg}.
- This study can be extended in the future to include the case of variable magnetic field, flow through a thermal non-equilibrium porous medium and other types of PCM.

- **Practical Implications** :

- Understanding the interplay between mixed convection, phase change, and magnetic fields could aid in designing more efficient heat exchangers or chemical reactors.
- The studied configuration could be adapted for cooling electronic components, with the PCM providing thermal inertia.
- Magnetic fields could be used to control melting rates, potentially allowing for more precise thermal management.

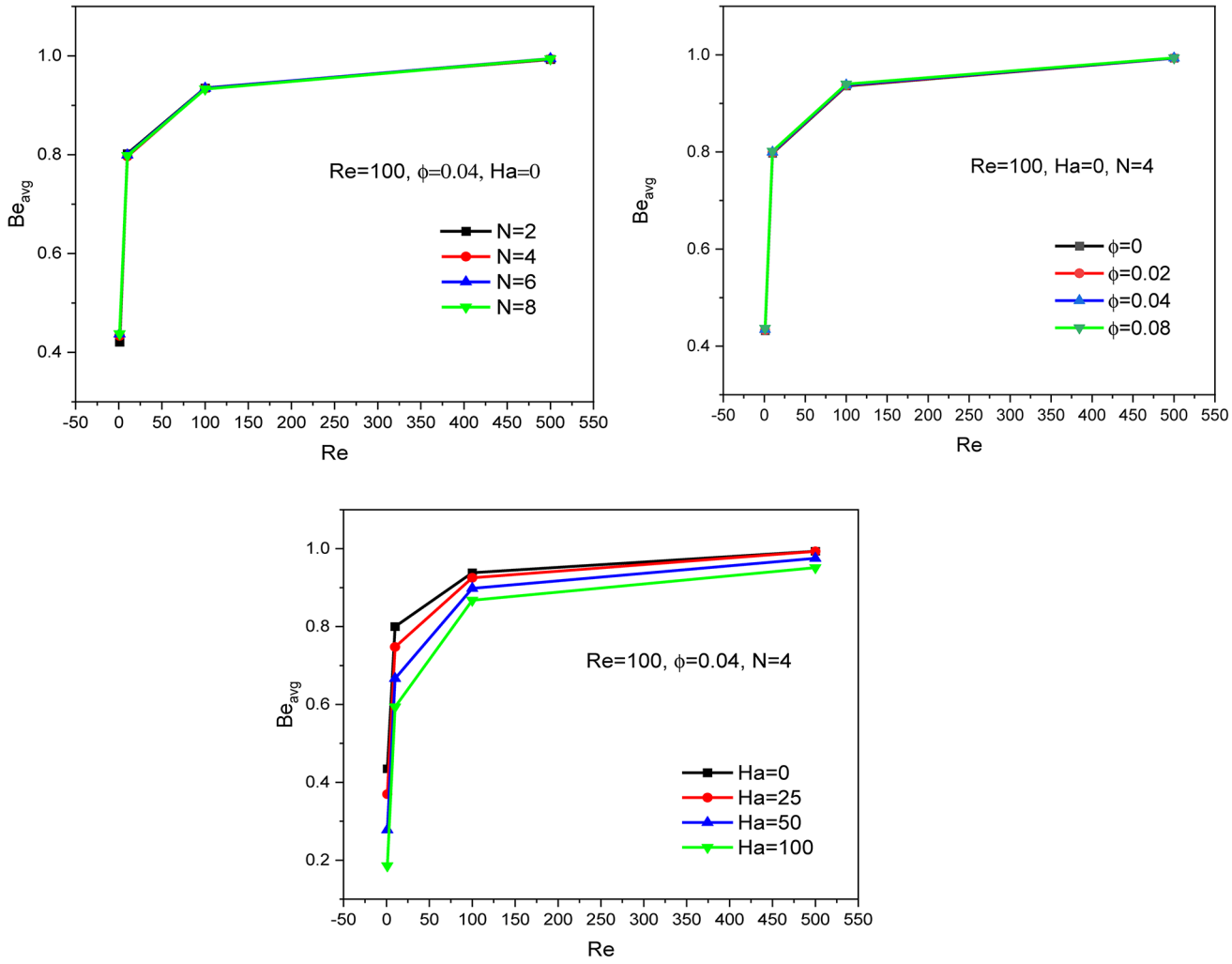


Fig. 7. Impact of the variations of Re, Ha, and φ on Be_{avg}.

Data availability

The datasets used and/or analysed during the current study available from the corresponding author on reasonable request.

Received: 4 August 2024; Accepted: 21 November 2024
Published online: 28 November 2024

References

1. Al-Maghalseh, M. & Mahkamov, K. Methods of heat transfer intensification in PCM thermal storage systems: Review paper. *Renew. Sustain. Energy Rev.* **92**, 62–94. https://doi.org/10.1016/j.rser.2018.04.064 (2018).
2. Ahmed, S. E. et al. Enhanced heat transfer for NePCM-melting-based thermal energy of finned heat pipe. *Nanomaterials*, **12**(1). https://doi.org/10.3390/nano12010129 (2022).
3. Mourad, A. et al. Recent advances on the applications of phase change materials for solar collectors, practical limitations, and challenges: A critical review. *J. Energy Storage*. **49**, 104186. https://doi.org/10.1016/j.est.2022.104186 (May 2022).
4. Hansda, S., Pandit, S. K., Tony, W. H. & Sheu Thermosolutal discharge of double diffusion mixed convection flow with brownian motion of nanoparticles in a wavy chamber. *J. Therm. Anal. Calorim.* **147** (12), 7007–7029 (2022).
5. Hansda, S., & Pandit, S. K. Performance of thermosolutal discharge for double diffusive mixed convection of hybrid nanofluid in a lid driven concave–convex chamber. *J. Therm. Anal. Calorim.* **148** (3), 1109–1131 (2023).
6. Hansda, S. & Pandit, S. K. Thermosolutal hydromagnetic mixed convective hybrid nanofluid flow in a wavy walled enclosure. *J. Magn. Magn. Mater.* **572**, 170580 (2023).
7. Rathore, P. K. S., Shukla, S. K. & Gupta, N. K. Potential of microencapsulated PCM for energy savings in buildings: A critical review. *Sustain. Cities Soc.* **53**, 101884 (2020).
8. Huang, X., Zhu, C., Lin, Y. & Fang, G. Thermal properties and applications of microencapsulated PCM for thermal energy storage: A review. *Appl. Therm. Eng.* **147**, 841–855. https://doi.org/10.1016/j.applthermaleng.2018.11.007 (2019).
9. Peng, G., Dou, G., Hu, Y., Sun, Y. & Chen, Z. Phase change material (PCM) microcapsules for thermal energy storage, *Adv. Polym. Technol.* **2020** (2020).

10. Li, W. Q. et al. Microencapsulated phase change material (MEPCM) saturated in metal foam as an efficient hybrid PCM for passive thermal management: A numerical and experimental study. *Appl. Therm. Eng.* **146**, 413–421. https://doi.org/10.1016/j.applthermaleng.2018.10.006 (2019).
11. Li, Z. & Yuan, J. Phase change microcapsules with high encapsulation efficiency using Janus silica particles as stabilizers and their application in cement. *Constr. Build. Mater.* **307**, 124971. https://doi.org/10.1016/j.conbuildmat.2021.124971 (2021).
12. Gado, M. G. Thermal management and heat transfer enhancement of electronic devices using integrative phase change material (PCM) and triply periodic minimal surface (TPMS) heat sinks. *Appl. Therm. Eng.* **258**, 124504 (2025).
13. Baruah, J. S., Athawale, V., Rath, P. & Bhattacharya, A. Melting and energy storage characteristics of macro-encapsulated PCM-metal foam system. *Int. J. Heat. Mass. Transf.* **182**, 121993. https://doi.org/10.1016/j.ijheatmasstransfer.2021.121993 (2022).
14. Cheng, J. et al. Preparation and characterization of carbon nanotube microcapsule phase change materials for improving thermal comfort level of buildings. *Constr. Build. Mater.* **244**, 118388 (2020).
15. Ho, C. J., Chen, W. C. & Yan, W. M. Experimental study on cooling performance of minichannel heat sink using water-based MEPCM particles. *Int. Commun. Heat. Mass. Transf.* **48**, 67–72 (2013).
16. Eisapour, M., Eisapour, A. H., Hosseini, M. J. & Talebizadehsardari, P. Exergy and energy analysis of wavy tubes photovoltaic-thermal systems using microencapsulated PCM nano-slurry coolant fluid. *Appl. Energy*. **266**, 114849. https://doi.org/10.1016/j.apenergy.2020.114849 (2020).
17. Xu, T., Chiu, J. N., Palm, B. & Sawalha, S. Experimental investigation on cylindrically macro-encapsulated latent heat storage for space heating applications. *Energy Convers. Manag.* **182**, 166–177 (2019).
18. Maier, M., Salazar, B., Unluer, C., Taylor, H. K. & Ostertag, C. P. Thermal and mechanical performance of a novel 3D printed macro-encapsulation method for phase change materials. *J. Build. Eng.* **43**, 103124. https://doi.org/10.1016/j.jobe.2021.103124 (2021).
19. Xu, T. et al. Experimental and numerical investigation of a latent heat thermal energy storage unit with ellipsoidal macro-encapsulation, *Energy*, **238**, 121828. https://doi.org/10.1016/j.energy.2021.121828 (2022).
20. Yan, W. M., Siao, Y. H. & Kasaeiana, A. Transient thermal energy storage in partitioned enclosures packed with microencapsulated phase change materials. *Int. Commun. Heat. Mass. Transf.* **86**, 253–261 (2017).
21. Ghasemi, K., Tasnim, S. & Mahmud, S. PCM, nano/microencapsulation and slurries: a review of fundamentals, categories, fabrication, numerical models and applications. *Sustain. Energy Technol. Assessments*. **52**, 102084. https://doi.org/10.1016/j.seta.2022.102084 (2022).
22. Alehosseini, E. & Jafari, S. M. Micro/nano-encapsulated phase change materials (PCMs) as emerging materials for the food industry. *Trends Food Sci. Technol.* **91**, 116–128. https://doi.org/10.1016/j.tifs.2019.07.003 (2019).
23. Ghoghaei, M. S. et al. A review on the applications of micro-/nano-encapsulated phase change material slurry in heat transfer and thermal storage systems. *J. Therm. Anal. Calorim.* **145** (2), 245–268 (2021).
24. Peng, H. et al. A review on synthesis, characterization and application of nanoencapsulated phase change materials for thermal energy storage systems. *Appl. Therm. Eng.* **185**, 116326 (2021).
25. Li, W. et al. Nano-encapsulated phase change material slurry (Nano-PCMS) saturated in metal foam: A new stable and efficient strategy for passive thermal management. *Energy* **165**, 743–751. https://doi.org/10.1016/j.energy.2018.09.147 (2018).
26. Shehzad, S. A., Alshuraiaan, B., Kamel, M. S., Izadi, M. & Ambreen, T. Influence of fin orientation on the natural convection of aqueous-based nano-encapsulated PCMs in a heat exchanger equipped with wing-like fins. *Chem. Eng. Process. - Process. Intensif.* **160**, 108287. https://doi.org/10.1016/j.cep.2020.108287 (Mar. 2021).
27. Zadeh, S. M. H., Mehryan, S. A. M., Islam, M. S. & Ghalambaz, M. Irreversibility analysis of thermally driven flow of a water-based suspension with dispersed nano-sized capsules of phase change material. *Int. J. Heat. Mass. Transf.* **155**, 119796 (2020).
28. Ghalambaz, M., Groşan, T. & Pop, I. Mixed convection boundary layer flow and heat transfer over a vertical plate embedded in a porous medium filled with a suspension of nano-encapsulated phase change materials. *J. Mol. Liq.* **293**, 111432 (2019).
29. Ahmed, S. E. & Raizah, Z. A. S. Analysis of the entropy due to radiative flow of nano–encapsulated phase change materials within inclined porous prismatic enclosures: finite element simulation. *J. Energy Storage*. **40**, 102719 (2021).
30. Sadr, A. N. et al. Simulation of mixed-convection of water and nano-encapsulated phase change material inside a square cavity with a rotating hot cylinder. *J. Energy Storage*. **47**, 103606. https://doi.org/10.1016/j.est.2021.103606 (2022).
31. Agresti, F. et al. Nano-encapsulated PCM emulsions prepared by a solvent-assisted method for solar applications. *Sol Energy Mater. Sol Cells*. **194**, 268–275 (2019).
32. Heydarian, R., Shafii, M. B., Rezaee Shirin-Abadi, A., Ghasempour, R. & Alhuyi Nazari, M. Experimental investigation of paraffin nano-encapsulated phase change material on heat transfer enhancement of pulsating heat pipe. *J. Therm. Anal. Calorim.* **137** (5), 1603–1613 (2019).
33. Ghalambaz, M., Mehryan, S. A. M., Mozaffari, M., Hashem Zadeh, S. M. & Saffari Pour, M. Study of thermal and hydrodynamic characteristics of water-nano-encapsulated phase change particles suspension in an annulus of a porous eccentric horizontal cylinder. *Int. J. Heat. Mass. Transf.* **156**, 119792. https://doi.org/10.1016/j.ijheatmasstransfer.2020.119792 (2020).
34. Ghalambaz, M. et al. Free convective melting-solidification heat transfer of nano-encapsulated phase change particles suspensions inside a coaxial pipe. *Adv. Powder Technol.* **31** (11), 4470–4481. https://doi.org/10.1016/j.apt.2020.09.022 (2020).
35. Mehryan, S. A. M., Ghalambaz, M., SasaniGargari, L., Hajjar, A. & Sheremet, M. Natural convection flow of a suspension containing nano-encapsulated phase change particles in an eccentric annulus. *J. Energy Storage*. **28**, 101236. https://doi.org/10.1016/j.est.2020.101236 (2020).
36. Zhuang, Y. & Li, H. et al. Experimental study on the melting performance of magnetic NePCMs embedded in metal foam subjected to a non-uniform magnetic field. *Sol. Energy Mater. Sol. Cells*. **250**, 112077 (2023).
37. Sheikholeslami, M. Solidification of NePCM under the effect of magnetic field in a porous thermal energy storage enclosure using CuO nanoparticles. *J. Mol. Liq.* **263**, 303–315 (2018).
38. Xu, W., Huang, T. et al. Regulation mechanism of magnetic field on non-newtonian melting and energy storage performance of metal foam composite nano-enhanced phase change materials. *Int. J. Heat Mass Transf.* **200**, 123501 (2023).
39. Shi, E., Zonouzi, S. A. et al. Enhancement of the performance of a NePCM filled shell-and-multi tube thermal energy storage system using magnetic field: A numerical study. *Appl. Therm. Eng.* **178**, 115604 (2020).
40. Shahsavar, A., Godini, A., Sardari, P. T., Toghraie, D. & Salehipour, H. Impact of variable fluid properties on forced convection of Fe3O4/CNT/water hybrid nanofluid in a double-pipe mini-channel heat exchanger. *J. Therm. Anal. Calorim.* **137** (3), 1031–1043 (2019).
41. Ghalambaz, M., Chamkha, A. J. & Wen, D. Natural convective flow and heat transfer of nano-encapsulated phase change materials (NePCMs) in a cavity. *Int. J. Heat. Mass. Transf.* **138**, 738–749 (2019).
42. Al-Rashed, A. A. et al. Three-dimensional investigation of the effects of external magnetic field inclination on laminar natural convection heat transfer in CNT–water nanofluid filled cavity. *J. Mol. Liq.* **252**, 454–468 (2018).
43. Ghalambaz, M., Mehryan, S. A. M., Zahmatkesh, I. & Chamkha, A. Free convection heat transfer analysis of a suspension of nano–encapsulated phase change materials (NePCMs) in an inclined porous cavity. *Int. J. Therm. Sci.* **157**, 106503 (2020).
44. Aissa, A. et al. Natural convection within inversed T-shaped enclosure filled by nano-enhanced phase change material: Numerical investigation. *Nanomaterials*. **12**, 2917 (2022).
45. Aissa, A. et al. 2D MHD mixed convection in a zigzag trapezoidal thermal energy storage system using NePCM123270. *Nanomaterials* (2022).

46. Laidoudi, H. & Makinde, O. D. Computational study of thermal buoyancy from two confined cylinders within a square enclosure wifth single inlet and outlet ports. *Heat. Transf.* **50**, 1335–1350 (2021).
47. Maneengam, A. et al. Entropy generation in 2D lid-driven porous container with the presence of obstacles of different shapes and under the influences of Buoyancy and Lorentz Forces. *Nanomaterials* **12**, 2206 (2022).
48. Laidoudi, H. et al. Marzouki. Irreversibility interpretation and MHD mixed convection of hybrid nanofluids in a 3D heated lid-driven Chamber. *Nanomaterials* **12**, 1747 (2022).

Acknowledgements
The authors extend their appreciation to the Deanship of Research and Graduate Studies at King Khalid University for funding this work through Large Research Project under grant number RGP2/47/45.

Author contributions
A. A. Conceptualization, Methodology, Formal analysis, Writing the original manuscript, Writing the revised manuscript, data curation.O. Y. Project administration, Formal analysis, Writing the original manuscript, Writing the revised manuscript, Funding.S. A. Visualization, Formal analysis, Writing the original manuscript, Writing the revised manuscript, Software.A. M. Validation, Formal analysis, Writing the original manuscript, Writing the revised manuscript, Resources.Z. R. Formal analysis, Writing the original manuscript, Writing the revised manuscript.A. A. Formal analysis, Writing the original manuscript, Writing the revised manuscript.

Declarations

Competing interests
The authors declare no competing interests.

Additional information
Correspondence and requests for materials should be addressed to A.A.

Reprints and permissions information is available at www.nature.com/reprints.

Publisher's note Springer Nature remains neutral with regard to jurisdictional claims in published maps and institutional affiliations.

Open Access This article is licensed under a Creative Commons Attribution-NonCommercial-NoDerivatives 4.0 International License, which permits any non-commercial use, sharing, distribution and reproduction in any medium or format, as long as you give appropriate credit to the original author(s) and the source, provide a link to the Creative Commons licence, and indicate if you modified the licensed material. You do not have permission under this licence to share adapted material derived from this article or parts of it. The images or other third party material in this article are included in the article's Creative Commons licence, unless indicated otherwise in a credit line to the material. If material is not included in the article's Creative Commons licence and your intended use is not permitted by statutory regulation or exceeds the permitted use, you will need to obtain permission directly from the copyright holder. To view a copy of this licence, visit http://creativecommons.org/licenses/by-nc-nd/4.0/.

© The Author(s) 2024